Device

Article

Increasing power densities in a thermoelectric generator by stacking and incorporating dual heat pipes

Graphical abstract

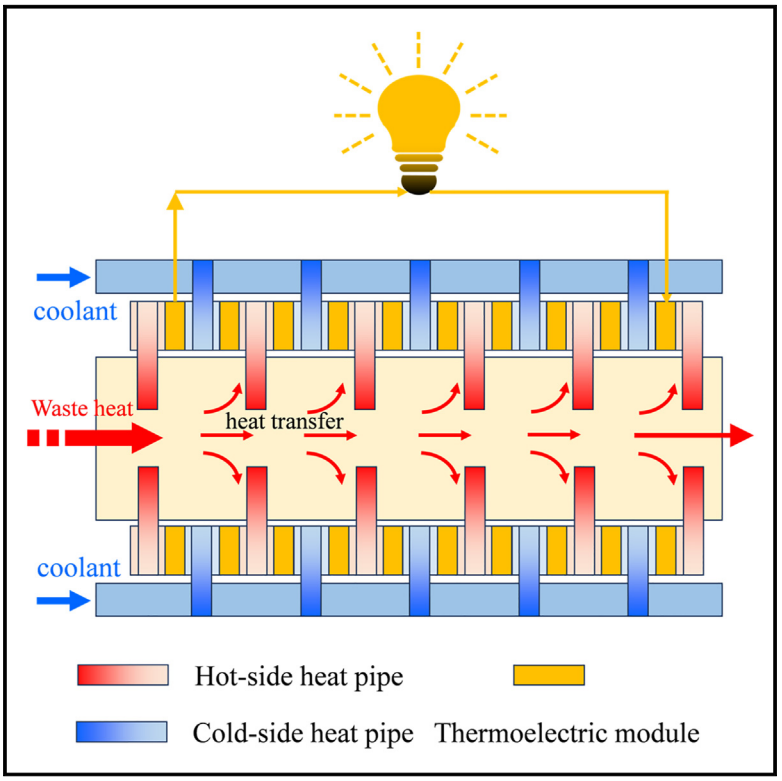

Authors

Ding Luo, Yuan Yu, Yuying Yan, Wei-Hsin Chen, Bingyang Cao

Correspondence

yu@physik.rwth-aachen.de (Y.Y.), caoby@tsinghua.edu.cn (B.C.)

In brief

A thermoelectric generator (TEG) prototype is created with 240 thermoelectric modules by combining a stacked design and heat pipes. Its performance is calculated through simulations and measured through experiments, with a power output of 848.37 W and a power density of 48.22 W L^{-1} at a temperature of 650 K and a flow rate of 50 m s^{-1}.

Highlights

- A stacked TEG achieved a power density of 48.22 W L^{-1}
- The effectiveness of heat pipes is demonstrated in experiments and simulations
- The importance of topology optimization is discussed and corroborated by simulations
- A power output of 848.37 W is achieved by the TEG prototype

4 Validate
Functional device with real-world testing, ready to scale

Luo et al., 2024, Device 2, 100435
July 19, 2024
https://doi.org/10.1016/j.device.2024.100435

CellPress

Please cite this article in press as: Luo et al., Increasing power densities in a thermoelectric generator by stacking and incorporating dual heat pipes, Device (2024), https://doi.org/10.1016/j.device.2024.100435

Device

CellPress
OPEN ACCESS

Article

Increasing power densities in a thermoelectric generator by stacking and incorporating dual heat pipes

Ding Luo,[1] Yuan Yu,[2,*] Yuying Yan,[3] Wei-Hsin Chen,[4,5,6] and Bingyang Cao[1,7,*]
[1]Key Laboratory for Thermal Science and Power Engineering of Ministry of Education, Department of Engineering Mechanics, Tsinghua University, Beijing 100084, China
[2]Institute of Physics (IA), RWTH Aachen University, 52074 Aachen, Germany
[3]Faculty of Engineering, University of Nottingham, University Park, Nottingham, UK
[4]Department of Aeronautics and Astronautics, National Cheng Kung University, Tainan 701, Taiwan
[5]Research Center for Smart Sustainable Circular Economy, Tunghai University, Taichung 407, Taiwan
[6]Department of Mechanical Engineering, National Chin-Yi University of Technology, Taichung 411, Taiwan
[7]Lead contact
*Correspondence: yu@physik.rwth-aachen.de (Y.Y.), caoby@tsinghua.edu.cn (B.C.)
https://doi.org/10.1016/j.device.2024.100435

THE BIGGER PICTURE The majority of heat from exhaust gas in vehicles and factories is released into the environment as waste. Thermoelectric power generation can capture this waste heat and turn it into useful energy. We report a thermoelectric generator (TEG) design using stacked TEGs with dual heat pipes that can more effectively extract heat from the exhaust gas and convert it to electricity. The introduction of heat pipes enables efficient heat transfer between heating/cooling sources and hot/cold sides of TEMs, as well as facilitates the integration of more TEMs in the limited space. During experiments, a power density of 48.22 W L^{-1} was observed for our design. This TEG prototype can be extended by altering the number of layers in a stacked structure, with each layer comprising 12 TEMs, a hot-side plate, a cold-side plate, 24 heat pipes, and six heat pipe covers, to adapt to a broad range of applications.

SUMMARY

Thermoelectric generators (TEGs) hold potential for waste heat recovery applications, but their ability to generate electricity within the confined space of exhaust systems remains a challenge. This work introduces a stacked TEG with dual heat pipes to facilitate heat transfer between thermoelectric modules and hot/cold sources and to help optimize space utilization. We also designed an apparatus to assess the output performance of TEGs. Our experimental findings reveal that, at a temperature of 650 K and a flow rate of 50 m s^{-1}, the stacked TEG can produce 848.37 W of electricity with a power density of 48.22 W L^{-1}.

INTRODUCTION

For fuel-powered engines, a considerable part of thermal energy is emitted into the surroundings along with the exhaust gas, resulting in serious issues of energy waste and CO_2 emission. Several waste heat recovery technologies have been developed to reuse this kind of waste heat, including the Rankine cycle,[1] Turbocharger,[2] and thermoelectric generator (TEG).[3] As a solid-state thermal-to-electric energy conversion technique, a TEG holds the advantages of small size, low noise, and long service life.[4–7]

In the automotive waste heat recovery field, numerous TEG devices are in use, with output power ranging from 100 W to 1 kW.[8–13] Crane et al.[9] designed a compact TEG using a special configuration of the Y-shaped thermoelectric module (TEM) and achieved a power output of 608 W and a power density of 42 W L^{-1} with a heat supply of 40.19 K kg s^{-1} (at a temperature of 620°C and a flow rate of 45 g s^{-1}). Zhang et al.[13] designed a stacked TEG with 400 TEMs, which could generate 1002.6 W with a 2.1% heat-to-electricity efficiency at a heat supply of 395.11 K kg s^{-1} (550°C and 480 g s^{-1}). The TEG has experienced a boost in output power through the heat transfer optimization of heat exchangers and the inclusion of more TEMs. Several heat exchanger optimization approaches, such as metal foam,[14] porous medium,[15] and advanced fin structure,[16] have been developed to enhance TEG performance, achieving an output power of 323.42, 119, and 612 W, respectively. Some special TEG configurations have also been proposed to introduce more TEMs and improve power density. For instance, a square shape,[17] hexagonal shape,[18] octagonal shape,[19] and stacked

Please cite this article in press as: Luo et al., Increasing power densities in a thermoelectric generator by stacking and incorporating dual heat pipes, Device (2024), https://doi.org/10.1016/j.device.2024.100435

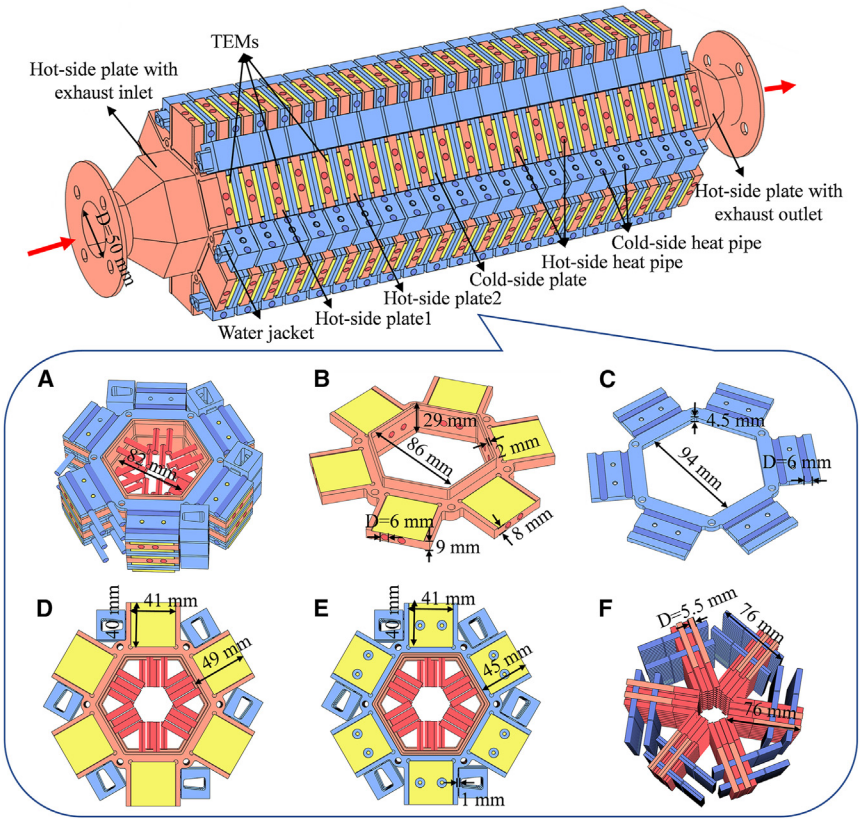

Figure 1. Schematic of the stacked TEG with dual heat pipes

(A) The stacked design.

(B) Hot-side plate 1.

(C) Cold-side plate.

(D) The combination of the hot-side plate with other components.

(E) The combination of the cold-side plate with other components.

(F) Hot-side and cold-side heat pipes.

design[20] enabled the incorporation of 34, 18, 306, and 224 TEMs within a limited space, achieving power densities of 16.29, 24.08, 2.50, and 34.67 W L^{-1}, respectively.

Although the mentioned technologies have improved performance, the performance degradation from the material level to the system level[21] and the overall low conversion efficiency of the TEG still limited its broader application and commercialization. Considering the low heat transfer performance from the exhaust gas to TEMs, researchers[22,23] adopted enhanced heat transfer methods to improve the heat-to-electricity efficiency of the TEG, including efficient fins,[24,25] heat pipes,[26,27] and phase change materials.[28] The reported heat transfer enhancement techniques[29] have, to some extent, improved the output performance of the TEG. However, for automotive waste heat recovery, the TEG is limited by the space available around the exhaust system and the increased pressure drop[10] due to the additional exhaust flow resistance. The use of heat pipes in the TEG is a promising way to enhance the output performance because of their high thermal conductivity; e.g., copper/water heat pipes can have a thermal conductivity of >18,000 W m^{-1} K^{-1}.[30–34] Additionally, heat pipes have the ability to alter the direction of heat flux, facilitating the design of TEG configurations. Compared with the traditional heat exchanger design with fins, the use of heat pipes can also alleviate the exhaust flow resistance, thereby reducing pressure drop.

We present a stacked TEG with dual heat pipes to improve power density in waste heat recovery. The developed TEG uses a stacked design to accommodate numerous TEMs and uses a hexagonal configuration to integrate the heat pipes to maximize heat transfer. On one end, the heat pipes extract heat from the exhaust gas and transfer it to hot-side plates. On the other end, the heat pipes transfer the heat of TEMs to the cooling water through cold-side plates. An experimental setup is used to test its performance under different conditions.

Device design and simulation

Design and assembly of the stacked TEG with dual heat pipes

Figure 1 presents the design and assembly of the stacked TEG with dual heat pipes, which consists of 21 hot-side plates (i.e., hot-side plate1, hot-side plate2, hot-side plate with exhaust inlet, and hot-side plate with exhaust outlet), 20 cold-side plates, 492 hot-side and cold-side heat pipes, 120 heat pipe covers, 6 water jackets, and 240 TEMs. Thanks to the high thermal conductivity of the heat pipe,[30] the use of dual heat pipes can ensure heat transfer from the exhaust to the TEM hot side and from the TEM cold side to the coolant.

Because of the stacked design, the expected power of the TEG can be adjusted by changing the number of TEMs, hot-side plates, and cold-side plates used, as shown in Figure 1A. From the exhaust inlet to the exhaust outlet, TEMs are divided into n (n = 1, 2, 3, …) rows, with each row including six TEMs. The Bi_2Te_3-based TEM (Figure S1; Table S1) with an overall size of 40 × 40 × 3.8 (length [L] × width [W] × height [H]) mm^3 is adopted. The thermoelectric properties of the p-type and n-type Bi_2Te_3-based bulk polycrystal materials are given in Figure S2. Here, a total of 40 TEM rows are used. Each row of TEMs is sandwiched between the hot-side plate and the cold-side plate (Table S2). Details for each component are as follows.

(1) Hot-side plate. Figure 1B presents the details of the hot-side plate 1, which has a hexagonal shape with six 40 × 41 mm^2 square slots, each with a depth of 0.5 mm to place the TEMs. On the edge of the hexagonal opening, there is a raised baffle with a height of 29 mm and a thickness of 2 mm. The thickness of the main body of the hot-side plate is 9 mm. Near the square slot, two circular holes

Please cite this article in press as: Luo et al., Increasing power densities in a thermoelectric generator by stacking and incorporating dual heat pipes, Device (2024), https://doi.org/10.1016/j.device.2024.100435

with a diameter of 6 mm are drilled from inside the hot plate, with a spacing of 13 mm, and the distances from the left and right borders of the slot are 10.5 mm and 17.5 mm, respectively. The circular holes are for inserting the hot-side heat pipes.

The hot-side plate is classified into two types: hot-side plate 1 and hot-side plate 2. The only difference between them lies in the inner tangential circle diameter, with the diameter of hot-side plate 1 and hot-side plate 2 being 86 mm and 82 mm, respectively. The two types of hot-side plates are assembled through baffles to form an exhaust flow channel. The circular holes between hot-side plate 1 and hot-side plate 2 are arranged in a staggered manner to ensure effective heat transfer between exhaust gas and heat pipes.

(2) Cold-side plate. The cold-side plate is composed of two similar sub-plates, with the cold-side heat pipe sandwiched between them, as shown in Figure 1C. The basic structure of the cold-side plate is similar to the hot-side plate, with six square slots at its six corners. At the position of the square slot, two semicircular holes with a diameter of 6 mm are excavated on the cold-side sub-plate, with a spacing of 20 mm, and the distances from the inner and outer borders of the slot are both 10 mm. After placing the cold-side heat pipes in the semicircular holes, the two sub-plates are fastened with screws to form the cold-side plate.

(3) Hot-side plates with exhaust inlet and outlet. The hot-side plates with exhaust inlet and outlet are formed by extension from the hexagonal baffle of the hot-side plates into a circular inlet and outlet. The diameter of the exhaust inlet and outlet is 50 mm to match the exhaust pipe.

(4) Heat pipe, cover, and water jacket. The heat pipes used in the hot-side and cold-side plates feature the same parameters, with a diameter of 5.5 mm and a length of 76 mm. Figure 1F shows the layout of heat pipes in the TEG prototype, where the hot-side pipes are arranged in a staggered manner. The heat of TEMs is dissipated into the cooling water through cold-side heat pipes. To achieve this goal, the cold-side pipes are inserted into the cubic covers with the size of 27 × 26 × 21 (L × W × H) mm^3. A trapezoidal through-hole and two circular holes with a diameter of 6 mm on both sides are excavated from the middle of the cover. The upper and lower bottom lengths of the trapezoidal through-hole are 8 mm and 12 mm, respectively, and the height is 20 mm. The distances of the trapezoidal through-hole from the upper and lower borders of the cubic cover are 2 mm and 4 mm, respectively. Here, the trapezoidal through-hole is used to place a water jacket, and the circular holes are used to place cold-side heat pipes. Besides, there is a small protrusion with a height of 1 mm at the top of the cover to avoid direct contact between the cover and the hot-side plate. The water jacket, in its cross-section, also exhibits a trapezoidal shape. Its upper base length matches that of the trapezoidal through-hole, but its height is smaller, measuring 18 mm. The cross section of the water jacket is smaller than that of the cover, aiming to ensure a snug fit. Besides, two 7-mm diameter water channels are incorporated within the water jacket.

(5) Assembly. Figures 1D and 1E show diagrams of the combination of the hot-side and cold-side plates with other components, respectively. 12 hot-side heat pipes are inserted into a hot-side plate to form a hot-side unit, and 12 cold-side heat pipes equipped with 6 covers are integrated into a cold-side plate to form a cold-side unit. The hot-side unit and cold-side unit are constantly stacked together, with 6 TEMs sandwiched between them. Then, the water jacket is placed in the trapezoidal through-holes of all covers, ultimately forming a stacked TEG with dual heat pipes.

Finite element simulations

Considering the space limitation of the exhaust system, we created a TEG prototype with 20 stacks and 240 TEMs in total, with a flange-to-flange length of 647 mm. The TEG can also be used for waste heat recovery in other applications (i.e., industrial and marine exhaust), and the number of stacks and overall size can be adjusted according to specific application scenarios. It is essential to verify the feasibility of the TEG through numerical simulations and bench tests before installing it on specific application objects. For this reason, finite element simulations were conducted to guide the performance analysis and experiments of the TEG prototype. To achieve this goal, a simulation method combining the computational fluid dynamics (CFD) model and thermal-electric model was developed.

The CFD model was employed to obtain the surface temperatures at both ends of the TEM. Subsequently, the temperature data were used as boundary conditions for the thermal-electric model to predict the TEM output. The simulation results are presented in Figure 2, with more details on boundary conditions and finite element model in Table S3 and Figure S3. The boundary conditions of the exhaust inlet refer to the application scenarios of waste heat recovery from automotive exhaust. All simulations were performed using the COMSOL Multiphysics software package. As shown in Figure 2A, there is a temperature drop along the exhaust downward flow direction, causing power loss when all TEMs are connected, especially in the full series topology connection. Due to the dual heat pipe design, a temperature difference is observed on both sides of the TEM during simulation, with the prediction for a power output. An oversized pressure drop from the exhaust inlet to the outlet may impact engine performance. For the TEG prototype, the generated pressure drop here is about 2.9 kPa (Figure 2B), which is lower than the reported value (4–8 kPa) in previous literature.[13,25] According to the simulation results, the proposed stacked TEG with dual heat pipes could generate more power with a smaller pressure drop.

Figures 2C–2F show the temperature distribution of a basic unit. The heat pipe transfers heat from the exhaust to the hot-side plate and from the cooling water to the cold-side plate. The TEMs located on the same layer have almost the same temperature distribution, as shown in Figure 2G. To compute the electrical output of TEMs, the average surface temperature on both sides of TEMs is extracted from CFD simulations and used as the boundary conditions of the thermal-electric numerical model. Figures 2H and 2I present the figure of merit (ZT) value and voltage distributions of a single TEM obtained by the thermal-electric numerical model,

Please cite this article in press as: Luo et al., Increasing power densities in a thermoelectric generator by stacking and incorporating dual heat pipes, Device (2024), https://doi.org/10.1016/j.device.2024.100435

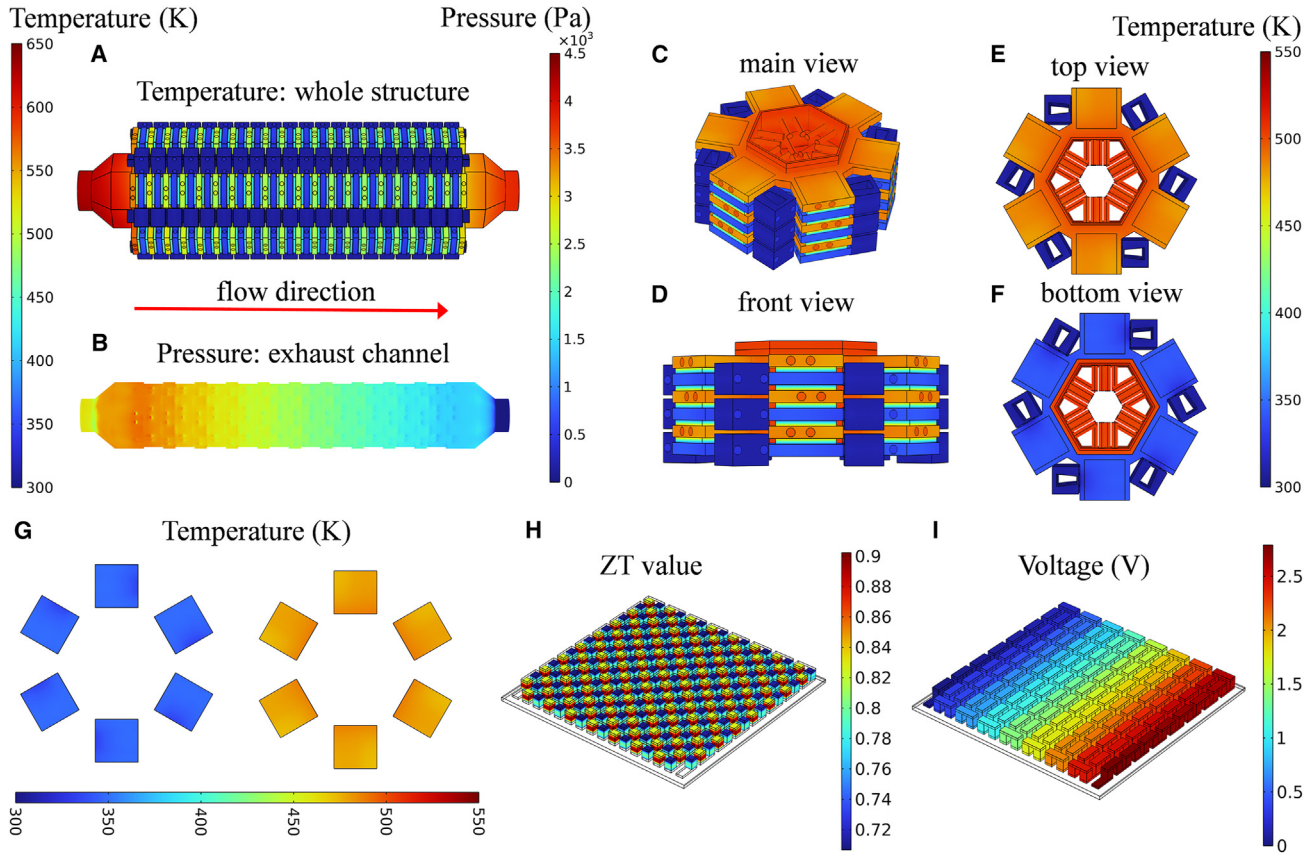

Figure 2. Finite element simulations of the TEG

(A) Temperature distribution of the whole structure.

(B) Pressure distribution of the exhaust channel.

(C–F) Main, front, top, and bottom views of the temperature distribution of the basic unit, respectively.

(G) Temperature distribution on the hot and cold sides of TEMs.

(H) ZT value of thermoelectric elements.

(I) Voltage distribution of the TEM.

respectively. The ZT value is temperature dependent, and p-type Bi_2Te_3-based materials have a larger ZT value than n-type materials, which shows the same trend as the material properties (Figure S2D). The electrical potential increment is in line with the series of thermoelectric semiconductors. Here, the output voltage is 2.79 V, and the used load resistance is 2 Ω. Through a simple calculation, the generated power of this single TEM is 3.89 W. Thus, the output power of TEMs, and even the entire TEG, can be predicted using this simulation method combining the CFD model and thermal-electric model.

Results and discussion

Fabrication process of the TEG prototype

Figure 3 shows a photo of the stacked TEG with dual heat pipes. The hot-side plate, cold-side plate, hot-side plates with exhaust inlet and outlet, cover, and water jacket are made of aluminum. The material of the heat pipe is copper, and the working fluid is water. The TEMs also use Bi_2Te_3 materials, with p-type $Bi_xSb_{2-x}Te_3$ materials by the alloy melting and spark plasma sintering methods and n-type $Bi_2Te_{3-x}Se_x$ materials by the hot pressing method. During the assembly process, thermal grease with a thermal conductivity of 6 W/(m•K) is applied between different components to prevent air gaps. Figures 3A–3D show the installation processes of the hot-side plate with heat pipes, cold-side heat pipes with covers, cold-side plate with heat pipes and covers, and the basic unit with hot-side plates, cold-side plates, TEMs, heat pipes, and covers. The assembly procedure begins with the hot-side plate with the exhaust inlet and progresses layer by layer until the entire TEG prototype is completed, as depicted in Figures 3E and 3F. Six screw rods pass through six positioning holes on the hot-side and cold-side plates, and the TEG stack is tightened together by the bolts and nuts. The water jacket and the cover are also secured through the screws on the cover. Given the intricate wiring throughout the TEG and the output of the six TEMs on the same layer, the wiring is organized using wire clips, and the six TEMs on the same layer are connected in series, as depicted in Figure 3G.

Experimental setup

To examine the performance of the fabricated TEG under different conditions, an experimental test bench is built, as shown in

Please cite this article in press as: Luo et al., Increasing power densities in a thermoelectric generator by stacking and incorporating dual heat pipes, Device (2024), https://doi.org/10.1016/j.device.2024.100435

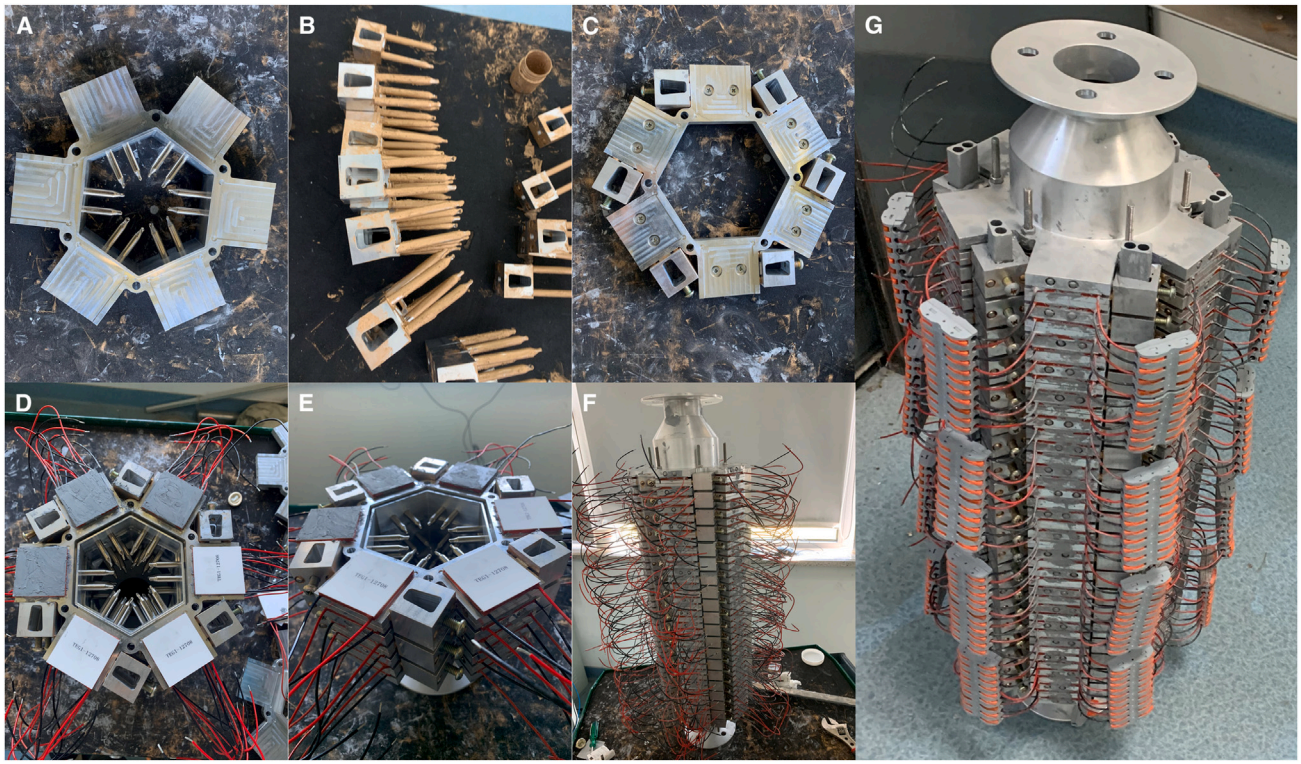

Figure 3. Prototype of the stacked TEG with dual heat pipes

(A) Hot-side plate with heat pipes.
(B) Cold-side heat pipes with covers.
(C) Cold-side plate with heat pipes and covers.
(D) Combination of hot-side plates, cold-side plates, TEMs, heat pipes, and covers.
(E) Assembly process.
(F) The assembled TEG prototype.
(G) The final TEG prototype after tightening and treatment.

Figure 4. Hot air and water are used as high-temperature exhaust gas and low-temperature coolant, respectively. The air blower (GB-2200s, Gebiao, China) is used to convey high-flow air into the heater (WR6000HT, Wellre, China). The high-temperature air enters and leaves the TEG prototype via the exhaust port. The water bath (DC-0530, Zhulan, China) is used to provide constant low-temperature water. Three K-type temperature sensors (SACIN-062U-6-SHX, Omega, USA) are incorporated into the exhaust inlet, exhaust outlet, and water pipe to measure temperatures. Temperature data are read and recorded by a data acquisitor (34970A, Keysight, China). An air velocity sensor (FMA1002B-V1, Omega) is installed in the air pipeline in front of the heater to measure the air velocity. Due to the maximum operating temperature of the air velocity sensor not exceeding 121°C, it can only be installed in front of the heater. The water flow rate is tested by a flow meter (SU7000, IFM, Germany), which is installed in the coolant pipeline. Here, the air blower, heater, air velocity sensor, and flow meter are all powered by the controller. Also, the designed controller is able to control the air velocity and air temperature through the built-in proportional integral differential (PID) control method. The produced electricity of the TEG prototype is measured by an electronic load (IT8513A+, Itech, China), which is connected to a computer and controlled by the computer to collect TEG electrical outputs at different resistances. Key information for the various apparatus is listed in Table S4.

Considering that the stacked TEG contains multiple layers of TEMs, as the hot air flows downward, a temperature drop will occur. When all TEMs are connected in series, the stacked TEG will experience electrical energy loss due to the uneven output of TEMs from different layers. For this reason, the impact of topological connection on the overall performance of the stacked TEG is studied first, where the TEMs are connected with different topological relationships. After obtaining the optimal topology connection, the effects of air temperature and air velocity on the output performance of the stacked TEG are measured. Considering the temperature limitation of the air heater and the velocity measuring limitation of the air velocity sensor, an air temperature range of 450–650 K and an air velocity range of 10–50 m s^{-1} are selected for experiments. The water temperature and flow rate are fixed at 288.15 K and 12 L min^{-1}, respectively. During the testing process, to obtain the maximum output power of the stacked TEG at different load resistances, the electronic load is controlled by the computer to gradually increase from 1 Ω to 800 Ω at an amplitude of 1 Ω and a frequency of 0.5 s.

Please cite this article in press as: Luo et al., Increasing power densities in a thermoelectric generator by stacking and incorporating dual heat pipes, Device (2024), https://doi.org/10.1016/j.device.2024.100435

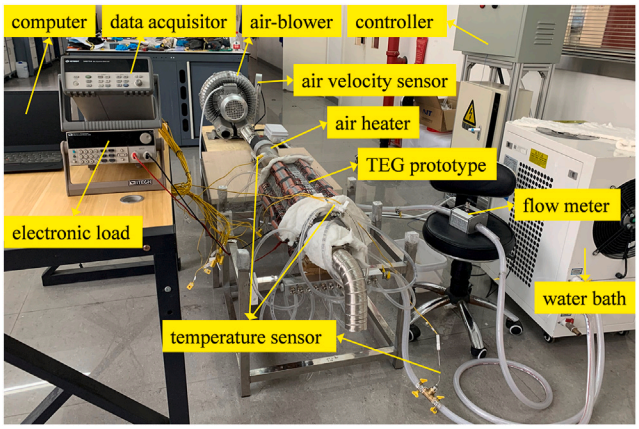

Figure 4. Experimental test bench for the TEG prototype

Topological optimization and experimental results

The stacked TEG contains 240 TEMs, and the topological connection between TEMs plays a role in the overall output, because the electrical output of TEMs at different layers is different. For example, if all TEMs are connected in series, then the overall output current of the TEG will be limited by the minimum current among TEMs. Consequently, TEMs between different layers are connected in a series/parallel hybrid manner, with TEMs in the same layer connected in series due to their identical temperature working conditions. A total of 40 layers are divided into N units, with each unit connected in series and different units connected in parallel. The first unit contains i layers of TEMs, the second unit contains $i + j$ layers, the third unit contains $i + 2j$ layers, and so on. N, i, and j are integers within the range from 1 to 40 and can be described by the following equation:

$$N \times i + \frac{N(N-1)}{2} j = 40 \qquad \text{(Equation 1)}$$

Four TEM topological relationships with relatively higher output performance are selected for comparative analysis and labeled case 1, case 2, case 3, and case 4, each corresponding to a different TEM topology connection manner (Figure S4 and Table S5). Figure 5A shows the TEG output power under four topological cases at an air temperature of 650 K and air velocity of 50 m s^{-1}. Case 3 features the highest output power, 848.37 W at R_L = 116 Ω, followed by case 2, case 1, and finally case 4. The relatively high output power in case 1 and case 2 only exists within a smaller range. In practical applications, the load resistance may fluctuate within a specific range. When the load resistance exceeds the optimal R_L operating range, the performance of the stacked TEG is severely damaged. Thus, case 1 and case 2 are not preferred. Compared with the traditional full series topology connection in case 4, the TEG output power using the optimized hybrid topology connection in case 3 is increased by 14.36%. Considering the highest output power and a large high-power operating range, case 3 is suggested.

Figure 5B shows the TEG output power under different air temperatures. Here, the air velocity is fixed at 50 m s^{-1}. When the air temperature increases from 450 K to 650 K, the maximum TEG power increases from 173.30 W to 848.37 W. In addition, the optimal load of the stacked TEG increases with increasing temperature. This is attributed to the temperature-dependent electrical resistivity[35] of thermoelectric materials, which leads to an elevation in the internal resistance of TEMs as the temperature increases. Figure 5C shows the volt-ampere (V-A) relationship of the stacked TEG under different air temperatures. The absolute value of the curve slope represents the internal resistance value of the stacked TEG. The output of the stacked TEG features the characteristics of low current and high voltage. At an air temperature of 650 K and the optimal load resistance, the output voltage and current reach 313.71 V and 2.70 A, respectively.

Air velocity also plays a role in the performance of the stacked TEG (Figures S5 and S6). The maximum TEG power improves from 120.69 W to 848.37 W as the air velocity increases from 10 m s^{-1} to 50 m s^{-1}. When the air velocity is low, the heat transfer between hot air and hot-side heat pipes remains low, resulting in the low hot-side temperature of TEMs. As the air velocity increases, the heat transfer becomes more intense, and hot-side heat pipes deliver more heat from the hot air to the TEMs. The voltage and the internal resistance of TEMs also increase with an increase in flow rate. At the maximum power point, with v_{air} = 10 m s^{-1}, the optimal load resistance for the stacked TEGs is 86 Ω, corresponding to a voltage of 101.88 V. However, when v_{air} = 50 m s^{-1}, the optimal load resistance becomes 116 Ω, and the voltage is increased by 208%. The output performance of the stacked TEG is highly sensitive to air temperature and flow rate, and the designed TEG is more suitable for application scenarios with higher temperatures and larger flow rates to generate electricity.

Power density

Figure 6 illustrates a power density comparison between our TEG prototype and similar devices in existing literature,[9,13–20,25,27] with different heat supplied (mass flow rate multiplied by temperature, $\dot{m} \cdot T$) and maximum power. Power density is defined as the ratio of maximum power to the physical volume occupied by the TEG from the exhaust inlet to the outlet (Figure S9). While the maximum power in this work, 848.37 W, is slightly lower than the 1002.6 W reported by Zhang et al.,[13] our setup only supplied a heat of 63.81 K kg s^{-1} compared to the 395.11 K kg s^{-1} in Zhang et al. Our TEG prototype can reach a power density of 48.22 W L^{-1}, which is higher than the reported values of 44.34 W L^{-1} in Zhang et al. and 42 W L^{-1} in Crane et al.[9] Other performance metrics of our prototype, such as coolant parameter and pressure drop (Table S6), also fare well compared to similar devices. For example, in this work, under a heat supply of 63.81 K kg s^{-1}, the pressure drop is only 2.88 kPa, which is lower than 8 kPa in Massaguer et al.[25] under a heat supply of 35.73 K kg s^{-1}.

Our TEG prototype has the potential to generate higher output when subjected to higher-grade heat inputs. Considering the limitations of the experimental apparatus with the maximum heat supply of 63.81 K kg s^{-1}, finite element simulations under different heat supplies were conducted to explore the relationship between heat supply and output power. As shown in Figure S7, the error in output power predicted by the simulation

Please cite this article in press as: Luo et al., Increasing power densities in a thermoelectric generator by stacking and incorporating dual heat pipes, Device (2024), https://doi.org/10.1016/j.device.2024.100435

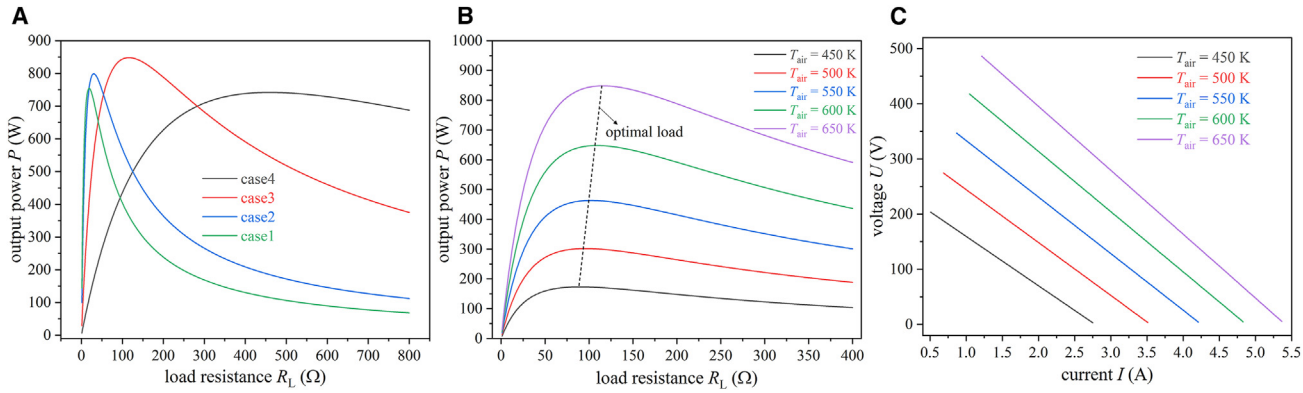

Figure 5. Topology optimization results and TEG performance at different temperatures

(A) TEG output power under four topological cases.

(B) TEG output power under different air temperatures.

(C) V-A curves under different air temperatures.

and experimental results is ~7%. The predicted relationship between the TEG performance and heat supply is presented in Figure S8. Considering that the working temperature of Bi_2Te_3-based thermoelectric materials shall not exceed 500 K, the TEG is expected to achieve a maximum power of 919.27 W and a power density of 52.25 W L^{-1} at this temperature. The proposed stacked design with dual heat pipes has the potential to generate higher electricity and higher power density by increasing the heat supply and improving the performance of thermoelectric materials.

Conclusions and outlook

In summary, we have presented a TEG design with high energy and power densities in waste heat recovery using a stacked design and the incorporation of heat pipes. An experimental setup has been established to carry out performance tests. Considering the performance degradation caused by temperature drop, the interconnection between TEMs was optimized before conducting large-scale experiments. Compared to a previous study,[18] where TEMs were connected in full series topology, our stacked TEG adopted an optimized series/parallel hybrid topology connection, which enabled lower electrical power loss and exhibited a 14.36% improvement in output power. The stacked TEG with dual heat pipes delivers an output power of 848.37 W at the air temperature of 650 K and air velocity of 50 m s^{-1}, and with an increased heat supply, it has the potential for even higher output performance. Notably, even with a relatively modest heat supply of 63.81 K kg s^{-1}, the developed TEG prototype achieves a record-high power density of 48.22 W L^{-1}.

The proposed strategy offers a new avenue for the next generation of TEGs in waste heat recovery. It is worth noting that commercial TEMs are used here, and our TEG prototype is expected to have a higher output performance when using TEMs with higher thermoelectric performance. Another limitation in our setup is the low working temperature of the Bi_2Te_3-based TEM. Thermoelectric materials with higher working temperatures, such as PbTe-based materials, would allow the TEG prototype to operate with a more powerful heat supply, resulting in higher output. From the perspective of heat transfer, there is a large temperature drop in the heat transfer process from exhaust waste heat to hot-side heat pipes. Some enhanced heat transfer methods, such as using finned heat pipes or embedding a closed circular pipe inside the exhaust flow channel, can further improve the output of our TEG prototype.

EXPERIMENTAL PROCEDURES

Resource availability

Lead contact

Requests for further information, data, and resources will be fulfilled by the lead contact, Bingyang Cao (caoby@tsinghua.edu.cn).

Materials availability

This study did not generate new unique reagents.

Data and code availability

The data that support the figures and findings of this study are available from the corresponding authors, B.C. or Y. Yu, upon request. The simulation files for the CFD model and thermal-electric model are uploaded to Zenodo and can be downloaded at https://zenodo.org/records/11350139.

Materials and methods

Thermoelectric properties

The p-type and n-type Bi_2Te_3-based thermoelectric materials from Sagreon (Wuhan, China) are prepared by alloy melting combined with spark plasma sintering and by the zone melting process, respectively. The density was tested by the Archimedes method. The electrical transport properties of bars with an approximate dimension of 2.5 × 2.5 × 14 mm^3 were measured by a Seebeck coefficient/electrical resistivity measuring system (ZEM-3, Advance Riko). The uncertainty of the Seebeck coefficient and electrical resistivity is about 7% and 3%, respectively. The thermal diffusivity (D) and specific heat (C_p) were measured by the laser flash method (LFA 457, Netzsch) and the thermal conductivity was calculated from the formula $k = D \cdot C_p \cdot d$. The uncertainty of the thermal conductivity is about 10%.

TEM fabrication

The Bi_2Te_3-based thermoelectric device uses copper sheets as the electrodes and uses an Al_2O_3-based ceramic substrate with a high thermal conductivity as the insulation plate at the cold and hot sides. The copper sheet is pasted on the ceramic substrate with a staggered pattern through the direct copper coating. Then, the p-type and n-type thermoelectric elements, with a dimension of 1.4 × 1.4 × 1.6 mm cut from the Bi_2Te_3-based thermoelectric materials, are connected in series in a sandwich structure (i.e., insulating Al_2O_3-based ceramic sheet/electrode/p-type and n-type thermoelectric elements/electrode/Al_2O_3-based

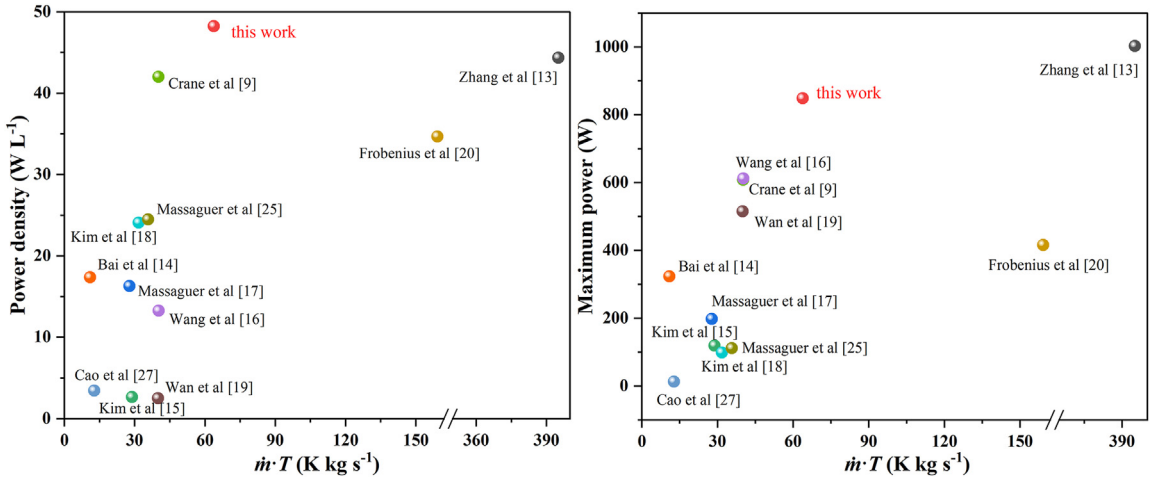

Figure 6. Comparison of power density of TEG prototypes between this work and published literature

ceramic sheet) by pressure welding. Besides, the welding surface of p-type and n-type thermoelectric elements was pre-plated with nickel to improve the wettability.

Simulation method

A coupling simulation model was developed to predict the performance of the stacked TEG with dual heat pipe. First, a CFD model was used to obtain the thermal distribution of the TEG, which was then used as input to the thermal-electric coupling model to calculate the output of TEMs. For the CFD model, the governing equations include

$$\nabla\cdot(\rho\vec{v}) = 0 \quad \text{(Equation 2)}$$

$$\nabla\cdot(\rho\vec{v}\vec{v}) = -\nabla p + \nabla\cdot(\mu\nabla\vec{v}) \quad \text{(Equation 3)}$$

$$\rho c\vec{v}\cdot\nabla T = \nabla\cdot(\lambda\nabla T) \quad \text{(Equation 4)}$$

$$\rho(\vec{v}\cdot\nabla)k = \nabla\cdot\left[\left(\mu+\frac{\mu_t}{\sigma_k}\right)\nabla k\right] + P_k - \rho\varepsilon \quad \text{(Equation 5)}$$

$$\rho(\vec{v}\cdot\nabla)\varepsilon = \nabla\cdot\left[\left(\mu+\frac{\mu_t}{\sigma_\varepsilon}\right)\nabla\varepsilon\right] + C_{1\varepsilon}\frac{\varepsilon}{k}P_k - C_{2\varepsilon}\rho\frac{\varepsilon^2}{k} \quad \text{(Equation 6)}$$

where Equations 2, 3, and 4 represent the conservations of mass, momentum, and energy, respectively. Equations 5 and 6 are the transport equations of the standard k-ε turbulent model. Under the given heat source input, these equations were solved using the finite element method on the COMSOL platform. Therefore, the surface temperature data of TEMs can be extracted from CFD results and used as input for the thermal-electric model.

For the thermal-electric model, the governing equations include

$$\nabla\cdot(\lambda_{p,n}(T)\nabla T) = T_{p,n}\vec{J}\cdot\nabla S_{p,n}(T) - \sigma_{p,n}^{-1}(T)\vec{J}^2 + \frac{\partial S_{p,n}(T)}{\partial T_{p,n}}T_{p,n}\vec{J}\cdot\nabla T \quad \text{(Equation 7)}$$

$$\vec{E} = -\nabla\varphi + S(T)\nabla T \quad \text{(Equation 8)}$$

$$\vec{J} = \sigma\vec{E} \quad \text{(Equation 9)}$$

$$\nabla\cdot\vec{J} = 0 \quad \text{(Equation 10)}$$

where Equation 7 represents the energy conservation of p-type and n-type thermoelectric elements. The first to third terms on the right side of Equation 7 represent Peltier heat, Joule heat, and Thomson heat, respectively. In the computing domain of copper electrodes, the first and third terms are absent, while in the computing domain of ceramic substrates, the first to third terms are all absent. Equations 8, 9, and 10 are the basic equations of the electrical field.

Similarly, under the boundary condition input of TEM surface temperature, Equations 7, 8, 9, and 10 were solved using the finite element method on the COMSOL platform, and the electrical output parameters can be extracted from the computational results.

SUPPLEMENTAL INFORMATION

Supplemental information can be found online at https://doi.org/10.1016/j.device.2024.100435.

ACKNOWLEDGMENTS

This project was supported by the National Natural Science Foundation of China (grants 52250273, U20A20301, and 52306017). The authors thank Dr. Yong Li and Wenguang Huang for providing the heat pipes, Dr. Xi'an Fan and Xiaoming Hu for providing the thermoelectric modules, and Dr. Guohua Wang for kind help with the construction of the experimental bench and prototype.

AUTHOR CONTRIBUTIONS

D.L. and Y. Yan conceived the idea. D.L. designed the experiments and contributed to the measurements. D.L. and Y. Yu wrote the manuscript. B.C. supervised the entire work. Y. Yu and W.-H.C. contributed to the review and revision.

DECLARATION OF INTERESTS

The authors declare no competing interests.

Received: April 1, 2024
Revised: April 22, 2024
Accepted: May 30, 2024
Published: June 26, 2024

REFERENCES

1. Laux, C., Gotter, A., Eckert, F., and Neef, M. (2022). Experimental results of a low-pressure steam Rankine cycle with a novel water lubricated radial inflow turbine for the waste heat utilization of internal combustion engines.

Energy Convers. Manag. *271*, 116265. https://doi.org/10.1016/j.enconman.2022.116265.

2. Feneley, A.J., Pesiridis, A., and Andwari, A.M. (2017). Variable Geometry Turbocharger Technologies for Exhaust Energy Recovery and Boosting-A Review. Renew. Sustain. Energy Rev. *71*, 959–975. https://doi.org/10.1016/j.rser.2016.12.125.

3. Luo, D., Sun, Z., and Wang, R. (2022). Performance investigation of a thermoelectric generator system applied in automobile exhaust waste heat recovery. Energy *238*, 121816. https://doi.org/10.1016/j.energy.2021.121816.

4. Zhang, Q., Liao, J., Tang, Y., Gu, M., Ming, C., Qiu, P., Bai, S., Shi, X., Uher, C., and Chen, L. (2017). Realizing a thermoelectric conversion efficiency of 12% in bismuth telluride/skutterudite segmented modules through full-parameter optimization and energy-loss minimized integration. Energy Environ. Sci. *10*, 956–963. https://doi.org/10.1039/C7EE00447H.

5. Hao, F., Qiu, P., Tang, Y., Bai, S., Xing, T., Chu, H.-S., Zhang, Q., Lu, P., Zhang, T., Ren, D., et al. (2016). High efficiency Bi2Te3-based materials and devices for thermoelectric power generation between 100 and 300 °C. Energy Environ. Sci. *9*, 3120–3127. https://doi.org/10.1039/C6EE02017H.

6. Bell, L.E. (2008). Cooling, Heating, Generating Power, and Recovering Waste Heat with Thermoelectric Systems. Science *321*, 1457–1461. https://doi.org/10.1126/science.1158899.

7. Kim, S.I., Lee, K.H., Mun, H.A., Kim, H.S., Hwang, S.W., Roh, J.W., Yang, D.J., Shin, W.H., Li, X.S., Lee, Y.H., et al. (2015). Thermoelectrics. Dense dislocation arrays embedded in grain boundaries for high-performance bulk thermoelectrics. Science *348*, 109–114. https://doi.org/10.1126/science.aaa4166.

8. Thacher, E.F., Helenbrook, B.T., Karri, M.A., and Richter, C.J. (2007). Testing of an automobile exhaust thermoelectric generator in a light truck. Proc. Inst. Mech. Eng. - Part D J. Automob. Eng. *221*, 95–107. https://doi.org/10.1243/09544070jauto51.

9. Crane, D., LaGrandeur, J., Jovovic, V., Ranalli, M., Adldinger, M., Poliquin, E., Dean, J., Kossakovski, D., Mazar, B., and Maranville, C. (2013). TEG On-Vehicle Performance and Model Validation and What It Means for Further TEG Development. J. Electron. Mater. *42*, 1582–1591. https://doi.org/10.1007/s11664-012-2327-8.

10. Shen, Z.-G., Tian, L.-L., and Liu, X. (2019). Automotive exhaust thermoelectric generators: Current status, challenges and future prospects. Energy Convers. Manag. *195*, 1138–1173. https://doi.org/10.1016/j.enconman.2019.05.087.

11. Ando Junior, O.H., Maran, A.L.O., and Henao, N.C. (2018). A review of the development and applications of thermoelectric microgenerators for energy harvesting. Renew. Sustain. Energy Rev. *91*, 376–393. https://doi.org/10.1016/j.rser.2018.03.052.

12. Liu, X., Deng, Y.D., Li, Z., and Su, C.Q. (2015). Performance analysis of a waste heat recovery thermoelectric generation system for automotive application. Energy Convers. Manag. *90*, 121–127. https://doi.org/10.1016/j.enconman.2014.11.015.

13. Zhang, Y., Cleary, M., Wang, X., Kempf, N., Schoensee, L., Yang, J., Joshi, G., and Meda, L. (2015). High-temperature and high-power-density nanostructured thermoelectric generator for automotive waste heat recovery. Energy Convers. Manag. *105*, 946–950. https://doi.org/10.1016/j.enconman.2015.08.051.

14. Bai, W., Yuan, X., and Liu, X. (2017). Numerical investigation on the performances of automotive thermoelectric generator employing metal foam. Appl. Therm. Eng. *124*, 178–184. https://doi.org/10.1016/j.applthermaleng.2017.05.146.

15. Kim, T.Y., Negash, A.A., and Cho, G. (2016). Waste heat recovery of a diesel engine using a thermoelectric generator equipped with customized thermoelectric modules. Energy Convers. Manag. *124*, 280–286. https://doi.org/10.1016/j.enconman.2016.07.013.

16. Wang, Y., Li, S., Xie, X., Deng, Y., Liu, X., and Su, C. (2018). Performance evaluation of an automotive thermoelectric generator with inserted fins or dimpled-surface hot heat exchanger. Appl. Energy *218*, 391–401. https://doi.org/10.1016/j.apenergy.2018.02.176.

17. Massaguer, A., Pujol, T., Comamala, M., and Massaguer, E. (2020). Feasibility study on a vehicular thermoelectric generator coupled to an exhaust gas heater to improve aftertreatment's efficiency in cold-starts. Appl. Therm. Eng. *167*, 114702. https://doi.org/10.1016/j.applthermaleng.2019.114702.

18. Kim, T.Y., Kwak, J., and Kim, B.-w. (2018). Energy harvesting performance of hexagonal shaped thermoelectric generator for passenger vehicle applications: An experimental approach. Energy Convers. Manag. *160*, 14–21. https://doi.org/10.1016/j.enconman.2018.01.032.

19. Wan, Q., Liu, X., Gu, B., Bai, W., Su, C., and Deng, Y. (2019). Thermal and acoustic performance of an integrated automotive thermoelectric generation system. Appl. Therm. Eng. *158*, 113802. https://doi.org/10.1016/j.applthermaleng.2019.113802.

20. Frobenius, F., Gaiser, G., Rusche, U., and Weller, B. (2016). Thermoelectric Generators for the Integration into Automotive Exhaust Systems for Passenger Cars and Commercial Vehicles. J. Electron. Mater. *45*, 1433–1440. https://doi.org/10.1007/s11664-015-4059-z.

21. Luo, D., Liu, Z., Yan, Y., Li, Y., Wang, R., Zhang, L., and Yang, X. (2022). Recent advances in modeling and simulation of thermoelectric power generation. Energy Convers. Manag. *273*, 116389. https://doi.org/10.1016/j.enconman.2022.116389.

22. Chen, W.-H., Wang, C.-M., Huat Saw, L., Hoang, A.T., and Bandala, A.A. (2021). Performance evaluation and improvement of thermoelectric generators (TEG): Fin installation and compromise optimization. Energy Convers. Manag. *250*, 114858. https://doi.org/10.1016/j.enconman.2021.114858.

23. Yan, S.-R., Moria, H., Asaadi, S., Sadighi Dizaji, H., Khalilarya, S., and Jermsittiparsert, K. (2020). Performance and profit analysis of thermoelectric power generators mounted on channels with different cross-sectional shapes. Appl. Therm. Eng. *176*, 115455. https://doi.org/10.1016/j.applthermaleng.2020.115455.

24. Luo, D., Yan, Y., Li, Y., Yang, X., and Chen, H. (2023). Exhaust channel optimization of the automobile thermoelectric generator to produce the highest net power. Energy *281*, 128319. https://doi.org/10.1016/j.energy.2023.128319.

25. Massaguer, A., Massaguer, E., Comamala, M., Pujol, T., González, J.R., Cardenas, M.D., Carbonell, D., and Bueno, A.J. (2018). A method to assess the fuel economy of automotive thermoelectric generators. Appl. Energy *222*, 42–58. https://doi.org/10.1016/j.apenergy.2018.03.169.

26. Wang, C., Tang, S., Liu, X., Su, G.H., Tian, W., and Qiu, S. (2020). Experimental study on heat pipe thermoelectric generator for industrial high temperature waste heat recovery. Appl. Therm. Eng. *175*, 115299. https://doi.org/10.1016/j.applthermaleng.2020.115299.

27. Cao, Q., Luan, W., and Wang, T. (2018). Performance enhancement of heat pipes assisted thermoelectric generator for automobile exhaust heat recovery. Appl. Therm. Eng. *130*, 1472–1479. https://doi.org/10.1016/j.applthermaleng.2017.09.134.

28. Catalan, L., Araiz, M., Aranguren, P., and Astrain, D. (2020). Computational study of geothermal thermoelectric generators with phase change heat exchangers. Energy Convers. Manag. *221*, 113120. https://doi.org/10.1016/j.enconman.2020.113120.

29. Zhao, G., Wang, X., Negnevitsky, M., and Li, C. (2023). An up-to-date review on the design improvement and optimization of the liquid-cooling battery thermal management system for electric vehicles. Appl. Therm. Eng. *219*, 119626. https://doi.org/10.1016/j.applthermaleng.2022.119626.

30. Solomon, A.B., Sekar, M., and Yang, S.H. (2016). Analytical expression for thermal conductivity of heat pipe. Appl. Therm. Eng. *100*, 462–467. https://doi.org/10.1016/j.applthermaleng.2016.02.042.

31. Zhao, Y., Fan, Y., Li, W., Li, Y., Ge, M., and Xie, L. (2022). Experimental investigation of heat pipe thermoelectric generator. Energy Convers. Manag. *252*, 115123. https://doi.org/10.1016/j.enconman.2021.115123.

32. Liu, Z., Cheng, K., Wang, Z., Wang, Y., Ha, C., and Qin, J. (2023). Performance analysis of the heat pipe-based thermoelectric generator (HP-TEG) energy system using in-situ resource for heat storage applied to the early-period lunar base. Appl. Therm. Eng. *218*, 119303. https://doi.org/10.1016/j.applthermaleng.2022.119303.

33. Li, T., Fu, Y., Dong, C., Li, D., Gu, H., and Ye, Y. (2023). Factors influencing the thermoelectric characteristics of a thermoelectric generator with cold-side micro heat pipe arrays. J. Power Sources *557*, 232493. https://doi.org/10.1016/j.jpowsour.2022.232493.

34. Kou, F., Wang, X., Zou, Y., and Mo, J. (2023). Heat transfer performance of the L-shaped flat gravity heat pipe used for zero-carbon heating houses. J. Build. Eng. *76*, 107389. https://doi.org/10.1016/j.jobe.2023.107389.

35. Witting, I.T., Chasapis, T.C., Ricci, F., Peters, M., Heinz, N.A., Hautier, G., and Snyder, G.J. (2019). The Thermoelectric Properties of Bismuth Telluride. Adv. Electron. Mater. *5*, 1800904. https://doi.org/10.1002/aelm.201800904.